Geophysical Journal International

New insights into North Sea deep crustal structure and extension from transdimensional ambient noise tomography

Journal:	*Geophysical Journal International*
Manuscript ID	GJI-S-20-0060.R1
Manuscript Type:	Research Paper
Date Submitted by the Author:	n/a
Complete List of Authors:	Crowder, Emily; University of Aberdeen Business School, School of Geosciences Rawlinson, Nick; University of Cambridge, Bullard Laboratories Cornwell, David; University of Aberdeen, School of Geology & Petroleum Geology Sammarco, Carmelo; AKKA Technologies Galetti, Erica; The University of Edinburgh, School of GeoSciences Curtis, Andrew; The University of Edinburgh, School of GeoSciences
Keywords:	Seismic tomography < SEISMOLOGY, Seismic noise < SEISMOLOGY, Crustal imaging < SEISMOLOGY, Crustal structure < TECTONOPHYSICS, Europe < GEOGRAPHIC LOCATION, Continental tectonics: extensional < TECTONOPHYSICS

New insights into North Sea deep crustal structure and extension from transdimensional ambient noise tomography

E. Crowder[1,*], N. Rawlinson[2], D. G. Cornwell[1], C. Sammarco[1], E. Galetti[3], A. Curtis[3,4]

1. School of Geosciences, University of Aberdeen, Aberdeen AB24 3UE, Scotland, United Kingdom
2. Department of Earth Sciences, University of Cambridge, Cambridge, CB3 0EZ, United Kingdom
3. School of Geosciences, University of Edinburgh, Edinburgh, EH8 9XP, United Kingdom
4. Institute of Geophysics, ETH Zurich, Zurich, Switzerland

Abbreviated title: Crustal S-wave velocity model of the North Sea from ambient seismic noise

* Corresponding author. Email address: emily.crowder@abdn.ac.uk (E. Crowder)

Summary

The deep crustal structure beneath the North Sea is poorly understood since it is constrained by only a few seismic reflection and refraction profiles. However, it is widely acknowledged that the mid to lower crust plays important roles in rift initiation and evolution, particularly when large scale sutures and/or terrane boundaries are present, since these inherited features can focus strain or act as inhibitors to extensional deformation. Ancient tectonic features are known to exist beneath the iconic failed rift system of the North Sea, making it an ideal location to investigate the complex interplay between pre-existing regional heterogeneity and rifting. To this end, we produce a 3D shear-wave velocity model from transdimensional ambient seismic noise tomography to constrain crustal properties to ~30 km depth beneath the North Sea and its surrounding landmasses. Major North Sea sedimentary basins appear as low shear-wave velocity zones that are a good match to published sediment thickness maps. We constrain relatively thin crust (13-18 km) beneath the Central Graben depocentres that contrasts with crust elsewhere at least 25-30 km thick. Significant variations in crustal structure and rift symmetry are identified along the failed rift system that appear to be related to the locations of Laurentia-Avalonia-Baltica paleo-plate boundaries. We constrain first-order differences in structure between paleo-plates; with strong lateral gradients in crustal velocity related to Laurentia-Avalonia-Baltica plate juxtaposition and reduced lower crustal velocities in the vicinity of the Thor suture, possibly representing the remnants of a Caledonian accretionary complex. Our results provide fresh insight into the pivotal roles that ancient terranes can play in the formation and failure of continental rifts and may help explain the characteristics of other similar continental rifts globally.

Keywords

Seismic tomography

Seismic noise

Continental tectonics: extensional

Crustal structure

Europe

1. Introduction

Continental regions subject to extensional stresses may eventually rift as the lithosphere becomes stretched and thinned. If extension continues, a continental rift can ultimately achieve full breakup and transition to seafloor spreading; yet this stage is often never reached, and a new mid-ocean rift does not form. The reasons why some rifts fail and others succeed are unclear; however, the mechanical strength and presence of pre-existing heterogeneity, including old sutures and faults, may be of primary importance. Understanding failed rift systems is crucial for understanding how plate tectonics operate on Earth more generally, but there is also an economic consideration in the form of the vast reserves of oil and gas that they host (e.g. Bass Strait, Australia; Benue Trough, Nigeria and the North Sea). While the structure of the uppermost crust and its extensional faulting, basin formation and hydrocarbon reservoirs tends to be well mapped and understood in these areas, below the economic basement the deeper crust remains poorly constrained. This is particularly true of the North Sea, where only a handful of vintage, deep seismic reflection/refraction profiles of varying quality have been collected and interpreted (e.g. Pharaoh, 1999). Yet, if we are to understand how rifts form and why they fail, it is crucial to be able to link upper crustal observations with mid-lower crustal properties and rift geometry, and their interaction, in order to assess the influence of pre-existing structures on rift initiation and evolution.

Prior to the formation of the North Sea, the northwest European Atlantic margin recorded a long and complex tectonic history. As summarised by Ziegler (1990), numerous extensional and orogenic events influenced the region since its initial formation during the triple plate collision of palaeo-continents in the Ordovician-early Devonian Caledonian Orogeny. This occurred when the Thor Ocean between Avalonia and Baltica closed by southward subduction under the north Avalonian margin (Torsvik and Rehnström, 2003). Subsequently, oceanic subduction switched northward beneath the Laurentian margin as Baltica-Avalonia moved towards Laurentia, closing the Iapetus Ocean in the late Silurian-early Devonian. Following the triple plate collision, there was widespread sedimentation in the Devonian as the newly formed Caledonian mountain ranges were eroded. Subsequently, extension in the Carboniferous resulted in crustal thinning, subsidence and successive sediment accumulation. From the Triassic to the Jurassic, most of Europe was subject to the main rifting stage of the North Sea and several kilometres of sediment accumulated in some basins. During the Cretaceous, rifting ceased, and subsidence slowed, creating the North Sea failed rift system as the dominant regional stresses shifted westward towards North America and the Proto-Atlantic opening (e.g. Afari et al. 2018). The location and continuity of ancient collisional sutures and spatial extent of old/deep extensional zones are uncertain and remain open to debate (e.g. Smit et al., 2016). Moreover, the failed rifting events in the North Sea overprint and therefore complicate interpretation of these older, but important crustal features.

To develop a better understanding of North Sea crustal structure and the potential interplay of ancient sutures and continental rifting, we use ambient noise tomography to create the first 3D shear-wave velocity model of the crust beneath the North Sea region. Prior to this work, the North Sea has been included in large-scale regional tomographic studies of Europe (e.g. Yang et al., 2007), where the horizontal resolution varies from ~100 km in the southernmost North Sea to >800 km in the central North Sea and is therefore only characterised by one or two broad scale velocity anomalies. In this study, we present a more detailed model of the crust to ~30 km depth in which numerous well-constrained features are recovered and interpret the new model in the context of the crustal structure and tectonic evolution of the region, with a particular focus on the relationship between ancient tectonic structures and lithospheric extension.

2. Data and methods

Prior to this study, surface wave velocities were found to be virtually impossible to extract from North Sea ambient noise data using conventional cross-correlation methods due to the high noise levels and complexities of the recovered signal (Galetti et al., 2016; Nicolson et al., 2014). However, by using recently developed processing techniques, we successfully obtain group velocity dispersion measurements, which are then used in a robust Bayesian, hierarchical, transdimensional tomography scheme to produce a new high-resolution model of the 3D shear-wave velocity structure beneath the North Sea.

Data for this study come from 54 permanent seismic stations located in countries surrounding the North Sea (Fig. 1). Both between and within the countries' networks there is high variability in terms of sample rate, type of instrument and corner frequency (which can limit the period range used in dispersion analysis). A major challenge for this dataset is the highly attenuative nature of the crust below the North Sea, which has previously been observed to dramatically reduce the signal-to-noise ratio of short (1-10 s) period surface waves (Ventosa et al., 2017). In the 1-2 s period range, it has been suggested that extremely high attenuation in the North Sea upper crust almost completely suppresses signal in ambient noise cross-correlations (Allmark et al., 2018). In this study, we have a minimum period of 4 s, thereby avoiding the attenuation problem at the shortest periods. Additional challenges arise from the dominant source of noise possibly being within rather than outside the study area (i.e. the Atlantic Ocean was assumed to be the main source, but the North Sea itself may be a significant contributor of microseismic noise – see Nicolson et al., 2014), which can produce spurious arrivals, and hence careful manual cross-checking of waveforms is required. If this is done properly, then this source heterogeneity will otherwise have little effect on narrow band traveltime measurements in ambient noise tomography (Yao & Van Der Hilst, 2009; Fichtner, 2014). In order to obtain high quality surface wave dispersion information, we use approximately five years of continuous data recorded between 2010 and 2015 and apply a new phase-weighted stacking technique (Ventosa et al., 2017), prior to carrying out ambient seismic noise tomography of the North Sea.

2.1. Preprocessing

The ambient noise cross-correlation procedure we employ is similar to that of Bensen et al. (2007), and utilises MSNoise (Lecocq et al., 2014) for data preprocessing. Continuous seismic recordings are split into hour long segments and carefully quality controlled by removing files containing glitches (e.g. data gaps or unexplained spikes) and/or data streams which are less than one-hour duration. To produce the highest quality empirical Green's functions, we first remove the mean, the trend and the instrument response from the noise recordings of vertical component traces. Subsequently, the mean and trend are removed again, and a taper is applied to each trace. The final corrected traces are merged to form files containing 24 hours of data (or at least 90% of one full day). All daily traces are down-sampled to a uniform 1 sps in order to perform daily cross-correlations.

2.2. Stacking

The daily cross-correlations and stacking processes are challenging aspects of this analysis largely due to the fact that the stations surround the North Sea, which itself is likely to be a major source of noise. This creates many artefacts in the cross-correlations that need to be excluded from further analysis. Tests on North Sea data show that phase cross-correlation (Schimmel et al., 2011) is the best approach for de-noising seemingly incoherent signals (Supplementary Fig. 1). To stack all the daily cross-correlations from the entire recording period for each station pair, time-domain phase weighted stacking (ts-PWS, Ventosa et al., 2017) was used (Supplementary Fig. 2). Phase-weighted stacking is a method based on analytic signal theory using the instantaneous phase at each given time on the signal envelope to optimally align traces (this is the phase that should be the same for coherent signals at each given time). When tested against the time-frequency domain PWS (Schimmel et al., 2011), results were very similar, but the ts-PWS was selected as the preferred method based on its significantly higher computational efficiency. A total of 1,275 empirical Green’s functions were successfully extracted from the 54-station network (Fig. 2).

2.3. Dispersion analysis

We performed group velocity dispersion measurements using a multiple filtering technique (via Computer Programs in Seismology software; Herrmann, 2013) applied to the symmetric component (stack of the causal and acausal signals) of the negative time derivative of the cross-correlation functions, which can be interpreted as Rayleigh wave empirical Green's functions. Group velocities were picked within a period range of 4 – 40 s (Fig. 3), and quality control is implemented via manual inspection of the 1,275 dispersion curves, which were categorised as "good", "fair" and "poor". The "poor" curves were deemed too noisy to pick. The "fair" curves were noisy, but dispersion maxima could be picked with low confidence. The "good" curves had the clearest group velocity dispersion maxima and could be confidently picked. Out of 760 picked dispersion curves, all 614 of the "good" curves are used in the subsequent inversion (Fig. 3). To investigate the feasibility of obtaining phase velocities we applied automated frequency-time analysis using the image transformation technique described in Young et al. (2011). However, the resultant phase dispersion plots were much noisier and less coherent than the equivalent group dispersion plots, which made reliable picking extremely challenging (see Supplementary Fig. 3).

2.4. Two-stage inversion

After making the group velocity measurements, a series of tomographic inversions were performed for even numbered periods between 4 and 40 s using the transdimensional, hierarchical Bayesian inversion technique described by Young et al. (2013). For each period of interest, the 2D group velocity model is dynamically parameterised by a tessellation of Voronoi cells, which adapt throughout the inversion to the spatially variable data coverage. The parameterisation is thus transdimensional in that the number, position, size and velocities of the cells are unknowns in the inversion and are implicitly controlled by the data. The approach is also considered hierarchical since the level of noise is treated as an unknown in the inversion process (Bodin et al., 2012). The aim is to quantify the posterior probability density distribution of all model parameters, conditional on the observed data. Out of 500,000 total iterations, model unknowns were assumed to have converged after the first 100,000, which were discarded as the "burn-in" phase. The remaining models were sifted by taking every 100th model, from which the average and standard deviation were calculated across a grid with a regular spacing of ~25 km in latitude and longitude (see Supplementary Material for full list of prior ranges and parameters). The final results of the inversion are represented by probability density functions with the average representing our “preferred” model and the standard deviation a measure of uncertainty. While ray trajectories are dependent on phase rather than group velocity, it is reasonable to expect that the correlation between phase and group velocity is stronger than between group and a constant velocity medium; hence we choose to use ray paths dictated by the group velocities rather than great circle paths. This assumption is commonly made in group velocity tomography (e.g. Bodin et al., 2012). Ray paths for periods 10, 20 and 30 s are shown in Fig. 4. With the exception of the region to the west of the Shetland Isles, and the other regions outside of our seismometer station network, there is generally excellent and even ray path coverage across the vast majority of the North Sea, especially at periods > 10 s, and therefore we are confident we sample the main tectonic features in the North Sea, albeit within the constraints of the horizontal and vertical resolutions inherent in the method.

With the set of period-dependent group velocity maps from the first stage of the inversion (Supplementary Fig. 4), we extracted velocity values at a regular grid of points across the study area in order to generate pseudo 1D group velocity dispersion curves at ~25 km spacing. These 2,903 curves were then independently inverted for 1D shear-wave velocity models by using a similar transdimensional, hierarchical Bayesian technique as described above, and subsequently merged together to create a full 3D model. The 1D shear-wave models are represented by a set of variable thickness layers, with the number, thickness and velocity of each layer free to vary during the inversion. The uncertainty estimates for the 2D group velocity maps were used to weight the input dispersion data in the 1D inversions. This ensures that noisy measurements (i.e. large standard deviation values) will not unduly influence the final solution. For each of the 2,903 pseudo-phase velocity dispersion curves, a total of 100,000 model iterations were produced with 50,000 discarded as "burn-in". We found that additional iterations did not significantly change the average 1D models. Shear-wave velocity was permitted to vary between 1.5 and 5.0 km/s, and the total number of layers between 2 and 20, although the natural parsimony of the transdimensional, hierarchical, Bayesian inversion means that the method tends towards a conservative solution, so an overestimation of velocity amplitudes is unlikely. The average and standard deviation of each 1D model was used to construct the final 3D solution model and its associated uncertainty.

2.5. Solution quality and synthetic resolution tests

To assess the reliability of group velocity maps produced by the 2D Bayesian inversion method, we performed a series of resolution tests based on synthetic data. In order to illustrate the potential recovery of velocity discontinuities and structure at different scales, we applied the so-called synthetic “checkerboard test”. This involved using an identical source-receiver path configuration to the observational dataset to predict travel-time residuals for a predetermined checkerboard structure defined by a pattern of alternating high and low velocity anomalies. Here, we assessed three checkerboard sizes: small (2.5º x 1.5º); medium (4.0º x 2.5º); and large (5.5º x 3.5º), with maximum perturbations of the synthetic velocity anomalies of ±0.5 km/s. Gaussian noise with a standard deviation equal to 1 s was added to the synthetic data to simulate uncertainties associated with the observational dataset (e.g. picking of group arrival time as a function of period). We used identical source–receiver path combinations to the observational dataset at 10, 20 and 30 s periods; the input structure for each of the three checkerboard sizes are shown in Fig. 4 (left column). The inversion was then carried out using the transdimensional, hierarchical Bayesian scheme.

The quality of the recovered checkerboard pattern is generally good (Fig. 5), with reasonable recovery of the input amplitudes, bearing in mind that there is no regularisation or preconditioning of the parameterisation (e.g. using the same grid spacing for the synthetic and recovered models) that is common in conventional linearised methods. By calculating the peak of each output checkerboard divided by the peak of each input checkerboard, within the North Sea the smallest size checkerboard test recovers ~55-85%, and the largest checkerboard test recovers ~65-100%, of the input amplitudes. Smearing of the velocity model is evident in some places, particularly in regions peripheral to the bounds of the receiver array. For example, the poor resolution in the north-western corner of the array is due to the station configuration, with only a single isolated receiver on the Faroe Islands that is somewhat removed from the rest of the array. However, across the North Sea itself there is some smearing in both NW-SE and NE-SW directions, but the distortion it causes is not severe. Overall, the checkerboard tests demonstrated that data from the 54 stations used in this work are capable of resolving features ~170 km in size with even better recovery in regions of the model with concentrated path coverage where we might expect smaller features to be better resolved (Fig. 5).

In order to investigate the reliability of the second stage of the transdimensional, hierarchical, Bayesian inversion, in which pseudo-group-velocity dispersion curves are inverted for 1D shear velocity models, we performed another synthetic test. A four-layer crustal shear wave velocity model which includes a low velocity layer was used as the synthetic input to test the ability of the inversion to recover structure, with Gaussian noise of 0.2 km/s standard deviation added to the group dispersion data to simulate measurement uncertainty. The quality of the recovered 1D shear velocity model is generally good; the probability density plot and its mean are in approximate agreement with the input model (Fig. 6), although the largest inconsistencies between the synthetic and recovered model occur in the neighbourhood of the velocity discontinuities. Given that surface waves cannot discriminate between velocity discontinuities and strong velocity gradients, the fact that the mean solution model produces a smoothed version of the layered input model is to be expected.

3. Results

We present the 3D crustal structure beneath the North Sea region in a series of horizontal and vertical slices taken from the final tomographic solution. Significant velocity anomalies that will be interpreted later are numbered on the horizontal slices in Fig. 7. We use the standard deviation of the model ensemble, computed at each individual grid point in latitude, longitude and depth, as an estimate of uncertainty (Fig. 8). Regions of high standard deviation can generally be correlated with a lack of path coverage or lack of crossing paths. Because there are no seismic stations beneath the oceans, uncertainty is in general higher offshore compared to onshore. In the following we quote Moho depths based upon the 4.2 km/s contour in our model; the accuracy of our Moho depth estimates will vary according to model uncertainty (Fig. 8) and the sharpness of the S-wave velocity gradient at the base of the crust. A proxy for depth uncertainty that we consider is the average difference between the 4.2 km/s contour and the 4.1 km/s and 4.3 km/s contours. Under this assumption, in offshore regions with a sharp Moho discontinuity a depth uncertainty of +/- 2 km is appropriate, whereas onshore with gentler Moho velocity gradients (where we sample the base of the crust) it is likely to be at least +/- 4 km.

Fig. 7(a) shows a horizontal slice at 4 km depth, which is dominated by low shear-wave velocities across the North Sea. These velocities, which vary between 2.2 and 2.9 km/s, are widespread across northern Germany, the Netherlands, Denmark and through the Central North Sea towards and beyond Shetland and Norway (labelled ‘1’). A notable area of higher velocity between the lows in the North Sea is a region with velocities of ~3.5 km/s to the east of northern England (labelled ‘2’). At 8 and 11 km depths (Fig. b-c), velocities of 2.8-3.1 km/s span much of the North Sea between the UK and Denmark. This relatively low velocity feature appears to terminate at the UK coastline, but may extend onshore in the east across northernmost Germany (labelled ‘3’). The horizontal slice at 15 km depth (Fig. 7d) also shows this low velocity anomaly, but here it is confined to the western part of the North Sea, adjacent to the UK. This implies that the anomaly could thicken and/or dip westward. At the eastern end of the depth slices at 11 and 15 km depth (Figs. 7c-d) is an area of elevated velocity in the vicinity of Denmark and southern Sweden (labelled ‘4’). It is characterised by velocities of ~4.1 km/s compared to its surroundings of ~3.8 km/s. Fig. 7(d-f) shows horizontal slices at 15, 20 and 25 km depth, on which we observe a pronounced zone of velocities >4.1 km/s that extend and widen northwards from the centre of the North Sea (labelled ‘5’). This zone is generally surrounded by lower velocities of ~3.5-3.8 km/s. At 25 km depth (Fig. 7f), this high velocity region appears to widen south of the centre of the North Sea; for example, at ~56º N it widens from ~170 km at 20 km depth, to ~360 km at 25 km depth. This widening is greater in the west of the velocity anomaly than the east. It also broadens with depth further north, where at 59º N the elevated velocities extend from ~215 km wide at 20 km depth, to ~295 km wide at 25 km depth. At depths of 20 and 25 km (Fig. 7e-f) a second region of very high velocities (>4.1 km/s) is present below northern Germany (labelled ‘6’). There appears to be a connection between the high velocities in the northern and central North Sea and those below northern Germany in a narrow (~100 km) ~N-S trending zone which features velocities of ~4.2 km/s.

Fig. 9(a) shows a vertical slice through our 3D shear velocity model taken at 60º N, which extends from the west of Shetland to eastern Norway. Assuming crustal velocities are generally <4.2 km/s (Kennett et al., 1995), we observe thin (~14 km) crust below the Viking Graben. Overlying the thinnest sections of crust, low velocities (<2.7 km/s) span the North Sea upper crust from Shetland to Norway (anomaly ‘1’). We also observe that the crustal velocity character is significantly different on either side of the thin region. Below Norway, crustal thickness is likely to be >30 km whereas below the Shetland Plateau it is ~27 km. Furthermore, on the Norwegian side the velocity properties are apparently more uniform with higher velocities (mostly >3.4 km/s) throughout, whereas on the Shetland side lower velocities are more extensive (~3.0 km/s in the upper crust). A vertical slice through our shear velocity model further south at 56º N (Fig. 9c) highlights other significant features in our results. Again, assuming a base of crust velocity of 4.2 km/s, we observe that the crustal thickness below central Scotland is ~30 km, which is in contrast to Denmark and Sweden where mantle velocities are not reached, implying a crustal thickness of >30 km. Low velocity anomaly ‘3’ is visible below the North Sea on this vertical slice. These velocities are lower than anywhere else in our model at these depths. This low velocity anomaly has an apparent westward dip or alternatively thickens to the west but does not continue below Scotland. The final key feature to note in this cross-section is the asymmetry of the highly elevated mantle velocities (>4.3 km/s, labelled ‘5’), which underlie the thin crust below the North Sea (Figs. 9a & 9c). We observe that these high velocities have a much more abrupt transition to normal crustal velocities in the east compared with the more gradual transition on the Scottish side.

4. Discussion

In this section we focus on key features and regions in the new 3D shear-wave velocity model that are relevant in addressing the link between lithospheric extension and pre-existing structures, which is the main goal of this study. We have taken care when interpreting features in our velocity model, particularly in regions where resolution is reduced and uncertainty is higher (e.g. Figs. 5 & 8), and focus the majority of our discussion on the deep crust where the velocity model is best resolved.

4.1. Sedimentary basins and the Mid North Sea High

In the uppermost crust, shear-wave velocities of 2.2-2.9 km/s are widespread across northern Germany, the Netherlands, Denmark and throughout the North Sea (labelled ‘1’ on Fig. 7a). These low velocities are characteristic of sedimentary basins, typically created by lithospheric extension, and we find their distribution matches well with sediment thickness maps, such as EuCRUST-07 (Tesauro et al., 2008), which is derived from seismic reflection, refraction and receiver function data. However, EuCRUST07 differs markedly from our model in the vicinity of the Mid North Sea High (MNSH), which lies in the Central North Sea between the Northern and Southern Permian Basins and has acted as a relative high since at least Devonian times (e.g. Arsenikos et al., 2019). Here, a distinct area of higher velocity (~3.5 km/s) is observed on the 4 km depth slice of our new model (anomaly ‘2’; Fig. 7a & 9c), which extends from the northeast coast of England and across the MNSH (Fig. 1), and appears to be confined to the uppermost ~5 km of the crust (Fig. 9c). Gravity studies have been used to map the presence of granites across the area (Wernicke, 1985) and Well 37/25-1 (drilled in 2009 by Esso) penetrated the Dogger High, and found that the crustal blocks likely contain granite cores, which typically exhibit higher shear-wave velocities than the surrounding sedimentary basins. This is especially true if shallow-level crustal intrusions are emplaced and grow through the incremental stacking of sill-like sheets, rather than isolated plutons (e.g. Wilson et al., 2016). The presence of granite throughout the MNSH uppermost crust is therefore a plausible explanation for the elevated velocities in this region. The size of each individual granite pluton is likely to be below the resolving power of our dataset, which may help explain why we observe a diffuse zone of elevated wavespeed (Fig. 5). Another consideration is that several boreholes on the MNSH sampled sedimentary rocks that experienced greenschist and possibly amphibolite facies metamorphism during late Ordovician times (Pharaoh et al., 1995). The laboratory estimated shear-wave velocity of greenschist is 3.57 km/s (Christensen, 1996), which is very close to the ~3.5 km/s shear-wave velocity we find in our model. We therefore suggest that a combination of granite-cored fault blocks and greenschist facies metamorphism explains the widespread elevated S-wave velocities we observe in the upper crust around the MNSH.

4.2. Low velocities in the mid-crust

A significant volume of unexpectedly low velocities (2.8-3.1 km/s) spans much of the North Sea between Denmark and the UK, adjacent to the Viking and Central Grabens, and best identified on the 11 km depth slice (anomaly '3'; Fig. 7c). This relatively low velocity zone appears to terminate at the eastern UK coastline and is also present on the horizontal model slice at 15 km depth (Fig. 7d), where it is confined to the western parts of the North Sea. On cross-section slice B-B' (Fig. 9c), anomaly '3' apparently extends to ~16 km depth, below which highly elevated velocities of >4.1 km/s exist, most likely indicating moderately thinned crust below it. We observe relatively higher standard deviation values (therefore greater uncertainty) in the offshore area, where anomaly '3' is located, than for the onshore area (Fig. 9c-d), and checkerboard resolution tests show that anomalies the size of '3' can be subject to a degree of smearing (Fig. 4e-h). However, this low velocity region is consistently present in our Rayleigh wave group period maps and subsequent S-wave velocity model.

A widespread low P-wave velocity mid-lower crust in the region of anomaly '3' has not been conclusively shown on previous seismic refraction/wide angle reflection profiles, largely because only a few sampled the fringes of this anomaly. 3D compilations of velocity models (e.g. Kelly et al., 2007) show a slightly elevated average crustal velocity in this region, but this is likely due to the absence of low velocity sedimentary rocks beneath the Mid North Sea High. However, a low (6.3-6.4 km/s) P-wave velocity zone in the mid- to lower crust either west of the Central Graben (Nielsen et al., 2000) or following the Caledonian Thor suture zone (Smit et al., 2016) was constrained on a number of deep seismic reflection and refraction profiles (i.e. MONALISA profiles 1–3 across the Central Graben; the combined European GeoTraverse sub-profiles EUGEMI and EUGENO-S 1 and LT-7, PQ-2; and BASIN-9601 profiles across the Baltica margin), but their locations do not constrain its westward extent. We find that our model exhibits low S-wave velocities in a similar location as the low P-wave anomalies described by Smit et al. (2016); however, the match is not perfect, and the low V_S region extends much further west. Based on the distribution of low V_S in our model, we propose that this low velocity zone continues much further westwards and could reach the British coastline. The low P-wave velocities were interpreted by Smit et al. (2016) as a separate crustal unit consisting of a collapsed Caledonian accretionary complex located between Baltica and Avalonia, who also compared it to the present-day Kuril and Cascadia subduction zones. In these modern cases, broad zones of low (6.4-6.6 km/s) P-wave velocities have been found in the subduction channels and interpreted to be due to either trapped fluids, highly sheared lower crustal rocks, and/or underthrust accretionary rock (e.g. Ramachandran et al. 2006). Further work that examines azimuthal anisotropy from Rayleigh waves, and radial anisotropy using a combination of Rayleigh and Love wave analysis may shed light on the internal properties of this anomaly.

Buried Devonian age or older sedimentary rocks may offer an alternative explanation for low velocities in the mid-lower crust (e.g. Arsenikos et al., 2019; Milton-Worssell et al., 2010); however, at depths of up to 16 km, sedimentary material is unlikely to remain un-metamorphosed by high pressures and temperatures. For example, assuming an average geotherm of 23ºC/km (Madsen, 1974), the temperature at 15 km depth would be ~345 ºC putting the rocks into the greenschist metamorphic facies zone (Yardley, 1989). The laboratory estimated shear-wave velocity of greenschist is 3.57 km/s (Christensen, 1996), making it an unlikely sole candidate for our low shear-wave velocity zone (2.8-3.1 km/s).

A number of deep seismic reflection profiles acquired across the North Sea (e.g. BIRPS and SNST83-7; Klemperer et al., 1991) show an unreflective upper- to mid-crust in the same region as our anomaly '3', and (in most cases) it occurs directly above highly reflective lower crust. The high reflectivity itself has been attributed to igneous intrusion but may also represent cross-cutting low-angle structures or other compositional heterogeneity (e.g. Klemperer et al., 1991). If magmatic intrusion followed by expulsion of water from local metamorphism has occurred (*cf.* the Rhine Graben, Wenzel and Sandmeier, 1992), it is possible that migrated fluids trapped in the mid- to upper crust contribute to the unusually low shear wavespeeds below the North Sea. Taking the low shear-wave velocity zone in our model of 2.8-3.1 km/s, and corresponding P-wave velocities of 6.3-6.4 km/s (Smit et al., 2016), this gives an elevated V_P/V_S ratio of approximately 2.2. Low aspect ratio microcracks saturated with incompressible fluid and high pore fluid pressure in laboratory experiments have been shown to have high V_P/V_S close to 2.2 (Wang et al., 2012) and the presence of brines in microcracks and fractures have been proven to exist to depths of at least 12 km at 190 °C and 9 km at 265 °C in the Kola (Russia) and KTB (Germany) boreholes respectively, where the presence of fluids correlated with and helped explain the lowered seismic velocities (Smithson et al., 2000). The implication for our study is that the presence of fluid and microcracks could be a contributing factor to the low shear-wave velocity zone. Further studies to characterise the anisotropy in this region may help to confirm this interpretation, with microcracks expected to open according to the predominantly NW-SE maximum compressive ambient stress field (Heidbach et al., 2010).

The Caledonian Orogeny involved the subduction of part of the Tornquist Sea basin beneath Avalonia (Pharaoh et al., 1995), and geophysical evidence indicates that at least two subduction zones were involved in this process, remnants of which are presently known as the Thor Suture and the Dowsing-South Hewett Fault Zone. The latter fault zone is a long-lived NW-SE trending crustal lineament (Fig. 1) and was reactivated throughout late Palaeozoic and Mesozoic times (Pharaoh, 1999). On deep seismic reflection data it separates crust of distinctly different seismic reflectivity character, and a south-westerly dipping reflector at the Moho and upper mantle has been mapped parallel to, and just coastward of the fault zone which may mark the location of an Ordovician subduction zone and/or crustal suture (Klemperer et al., 1991). The low velocity zone in our shear-wave velocity model appears to terminate at the Dowsing-South Hewett Fault Zone (within our resolution limits) and therefore it is plausible that the low velocity region (anomaly '3') is either constrained or caused by these two ancient subduction zones.

4.3. Variations in North Sea crustal thinning

One of the most striking features of the 3D shear-wave velocity model is a high velocity zone (>4.3 km/s) that is widest and constrained at ≤15 km depth beneath the northern North Sea (Fig. 7d), narrows southward before widening (with an eastward offset) into the central North Sea where it occurs at 15-20 km depth (Fig. 7e). These high velocities are likely to be the result of surface waves sampling the uppermost mantle, which can be defined seismically as shear-wave speeds >4.3 km/s (e.g. PREM; Dziewonski and Anderson, 1981; AK135; Kennett et al., 1995) and therefore the shape and characteristics of the region of velocity anomaly '5' (Figs. 7 and 9) can provide information about the thinned crust due to North Sea extension and its possible relationship(s) with pre-existing structures.

The main region of high velocities in the northern North Sea occurs directly beneath low velocities associated with sedimentary rocks within the Viking graben, as shown on cross-section A-A' (Fig. 9a). The crust is constrained to be ~14 km thick, in contrast to the >30 km and ~27 km to the east and west, respectively, and the width of the region of upper mantle S-wave velocities is likely to be in the region of 2-300 km. Higher model uncertainty beneath the Shetland Islands region precludes detailed interpretation, but we do not appear to reach >4.2 km/s and therefore interpret that the Moho defines a symmetrically thinned crust beneath the

Viking graben axis, albeit with differing crustal thicknesses representing Laurentia and Baltica margins (Fig. 10a). Further south, the central and southern North Sea rifts are characterised by a more laterally abrupt transition to lower velocities to the east, compared to a more gradual, dipping geometry to the west. This asymmetry in crustal structure is markedly different from that further north and can be clearly observed on cross-section B-B' (Fig. 9c). Striking observations of crustal thinning in these parts of the North Sea are the large lateral offset between near-surface low velocities delineating prominent sedimentary basins (e.g. Fig. 7b) and crustal complexity at the Avalonia-Baltica boundary. We therefore show, for the first time at this scale, significant changes in geometry along strike of the thinned crust of the North Sea rift system that appear related to the pre-existing juxtaposition of ancient paleo-plates. The symmetric thinning in the northern North Sea is in contrast to the asymmetric thinning in the central and southern North Sea, with the different styles most likely controlled by ancient paleo-continents in each location; i.e. extension in lithosphere of Baltica and Laurentia origin in the north led to symmetric thinning, while extension in lithosphere of Avalonia and Laurentia origin in the south resulted in asymmetric thinning and eventual termination of the North Sea failed rift system (Fig. 10).

At depths >20 km, a second region of very high velocities (>4.3 km/s) is present below northern Germany (anomaly '6'; Fig. 7f). At shallower depths, this is the approximate location of the late Jurassic to early Cretaceous age Lower Saxony Basin (Fig. 1). The elevated velocities that characterise anomaly '6' are very similar to those of anomaly '5', perhaps indicating that this is another area of thinned crust where mantle velocities are being sampled. Interestingly, there appears to be some connection between the fast velocities below the Central Graben and those below the Lower Saxony Basin in a narrow (~100 km wide) zone of ~N-S trending velocities of ~4.2 km/s (Fig. 7e-f). This zone is situated beneath the South-Central North Sea Graben and the eastern Netherlands, both areas of substantial Carboniferous-Jurassic igneous activity which was coincident with the initial development of the Proto-South Central North Sea Graben (Sissingh, 2004). Taking into consideration the resolution of our model (Fig. 5), we tentatively suggest that the spatial relationship between the igneous activity and elevated shear-wave velocity zone could indicate that we are observing the extension of the southernmost part of the North Sea failed rift system into northern Germany.

4.4. Deep crustal structure, thinning and structural inheritance

Structural inheritance is a property of continental lithosphere that focusses deformation along pre-existing structures, e.g. faults, shear or suture zones (e.g. Schiffer et al., 2019). The associated reactivation is primarily controlled by the compositional and mechanical properties of the pre-existing structures (e.g. Holdsworth et al., 2001). We use our new S-wave velocity model to examine the relationships between the major pre-extensional structures that are present in the North Sea, in particular the different paleo-plates and their boundaries, some of which are marked by major suture zones, and evidence for crustal thinning (Fig. 11).

Beneath the northern North Sea, crustal thinning is most pronounced adjacent to the presumably resistant Norwegian Baltic Shield and a region of thinned crust underlies the Viking Graben and Horda Platform to the east. Further west, thinned crust exists east of the Shetland Islands and notably north of the Shetland Platform, which may support the conclusion of Fazlikhani et al., (2017) that Devonian tectonic extension occurred over a wide region of the northern North Sea.

The southern extent of the thinnest crust in the northern North Sea changes geometry in the vicinity of where the Southern Uplands Fault (SUF), Hardangerfjord Shear Zone (HSZ) and possible westward extension of the Sorgenfrei-Tornquist Zone (STZ) congregate, with the locus of thinning apparently offset to the east in regions south of the STZ. The thinnest crust here varies in lateral extent but is consistent with, for example, the thinnest crust in the refraction/gravity/magnetic model (Transect 1) of Williamson et al., 2002, and it primarily occurs in a region defined by the STZ to the north, crust that may represent a remnant accretionary wedge related to the Thor suture (Smit et al., 2018) to the west and south and the Caledonian Deformation Front (CDF) to the east (Fig. 11). The enigmatic crust interpreted by Smit et al., (2018) as a remnant Thor suture accretionary wedge (RTAW) could alternatively represent a deformed and metamorphosed flake of Avalonia Microplate (Pharaoh et al., 1995), or an entirely exotic crustal terrane caught up along the Avalonia/Baltica suture (Coney et al., 1980). Interestingly, the Central Graben appears to occur in this crust, where it is underlain by moderately thinned crust but is notably to the west of where our model shows elevated deep velocities interpreted as the upper mantle at shallowest depths (~15-20 km). This relationship may indicate that the crustal ribbon containing the remnant Thor accretionary wedge may possess properties that facilitate brittle faulting whilst inhibiting ductile extension.

The southern extent of the Central Graben that marks the major crustal thinning of the Southern North Sea major crustal thinning, as defined by our interpreted mantle S-wave velocities, is coincident with where the RTAW (Smit et al., 2016), following the Elbe Line, changes to a more northwest-southeast orientation and hence becomes oblique to the more north-south axis of the southern North Sea rift (Fig. 11). Overall extension in the North Atlantic region during Mesozoic times was in an E-W to NW-SE direction (e.g. Ziegler, 1990), which could indicate that the RTAW's orientation was sub-optimal for rifting to propagate further southwards. Our S-wave velocity models show an absence of the wide region of high velocity anomalies at 20 km depth as the rift attempts to cross the RTAW, most likely indicating less crustal thinning (possibly confined to a ~100 km wide zone) and they reappear beneath the Lower Saxony Basin in northern Germany.

In relation to the distribution of paleo-plates in the North Sea, rifting appears to initially follow the path of least resistance, the weakness that was the suture zone between Laurentia and Baltica, evidenced by our new 3D velocity model. When it reached the triple plate collision junction, it changes rifting style, becoming more complex and displaying an offset between upper crust and whole crust extension (Fig. 10). Our new model shows that rifting was unable to continue to propagate very far into Avalonian lithosphere, likely because it possesses different mechanical properties that require greater tectonic forces to extend. Structural inheritance, and in particular the influence of paleo-plates, plays a key role in rifting and rift failure. For example, a rift can initially exploit the weakest part of the lithosphere at a paleo-suture zone. However, if a juxtaposed paleo-plate is mechanically stronger and hence is able to resist strain localisation, then the rift may cease to propagate and ultimately fail. Our results provide new evidence of how inherited lithosphere properties, such as suture zones and variations in mechanical strength, are a fundamental control on rift formation, style, propagation and termination.

5. Conclusions

We present the first 3D shear-wave velocity model of the North Sea region from ambient seismic noise tomography. Due to noise sources within the North Sea, previous studies have found it difficult to extract reliable inter-station group velocity dispersion data. However, by utilising time–frequency domain phase-weighted stacking to improve the signal-to-noise, we were able to successfully extract robust surface wave dispersion information. A transdimensional, hierarchical, Bayesian inversion method, which is highly data driven and requires minimal tuning of initial parameters, was then applied to invert for shear wave velocity. This approach accounts for heterogeneous data coverage, produces an ensemble of solution models and can constrain data uncertainty parameters. Our main findings include:

- Low velocities (<2.9 km/s) across much of the North Sea, Denmark, the Netherlands and northern Germany which are interpreted as signatures of the major North Sea sedimentary basins and match well with published sediment thickness maps;
- Relatively higher velocities (~3.5 km/s) in the upper crust of the Mid North Sea High region, typical of granites and greenschist and corresponding to locations of granites inferred from gravity anomalies;
- Anomalously low velocities (2.8-3.1 km/s) in the upper- to mid-crust in the vicinity of the Thor suture and across the southern North Sea, which could be interpreted as representing the remnants of a Caledonian accretionary complex. Alternatively, they may be caused by the presence of water (and/or microcracks) related to possible magmatic underplating in the area associated with Jurassic rifting in the North Sea;
- Relatively higher velocities in the vicinity of the Trans European Suture Zone (~4.1 km/s compared to its surroundings of ~3.8 km/s);
- Significantly elevated velocities (>4.2 km/s) representing thinned (13-18 km) crust beneath the Viking and Central Grabens. Rift style appears to be symmetric in the northern North Sea Viking Graben and strongly asymmetric in the Central Graben. This may be related to the location of the Laurentia-Avalonia-Baltica paleo-plates.
- Shallow high velocities (>4.2 km/s at 20 km depth, implying thinner crust) below Germany, with a tentative connection to the main North Sea rift system via a narrow N-S trending corridor of high velocities.

Finally, we find that both rifting style (symmetric vs. strongly asymmetric) and propagation ability varies across crust of different paleo-plate origins. We suggest that our new 3D shear-wave velocity model provides evidence of how inherited paleo-plate boundaries and suture zones play a fundamental role in the genesis, evolution and termination of failed continental rifts.

Acknowledgments

The work contained in this paper was conducted during a PhD study undertaken as part of the Natural Environment Research Council (NERC) Centre for Doctoral Training (CDT) in

601 Oil & Gas [grant number NEM00578X/1]. This work was performed using the Maxwell High
602 Performance Computing Cluster of the University of Aberdeen IT Service
603 (www.abdn.ac.uk/staffnet/research/hpc.php), provided by Dell Inc. and supported by Alces
604 Software. Plots were generated with the Generic Mapping Tools or GMT (Wessel et al., 2013).
605 We thank Nick Schofield and Tim Pharaoh for constructive conversations, which aided the
606 interpretation of our results, and Amy Gilligan for her insightful advice during preparation of
607 this manuscript. We also thank Richard England and an anonymous reviewer for their
608 comments on the original version of the manuscript.

609

610 **References**

Allmark, C., Curtis, A., Galetti, E., de Ridder, S., 2018. Seismic attenuation from ambient noise across the North Sea Ekofisk permanent array. Journal of Geophysical Research: Solid Earth 123, 8691–8710.

Arsenikos, S., Quinn, M., Kimbell, G., Williamson, P., Pharaoh, T., Leslie, G., Monaghan, A., 2019. Structural development of the Devono-Carboniferous plays of the UK North Sea. Geological Society, London, Special Publications 471, 65–90. https://doi.org/10.1144/SP471.3

Audet, P., Bostock, M.G., Christensen, N.I., Peacock, S.M., 2009. Seismic evidence for overpressured subducted oceanic crust and megathrust fault sealing. Nature 457, 76.

Bensen, G.D., Ritzwoller, M.H., Barmin, M.P., Levshin, A.L., Lin, F., Moschetti, M.P., Shapiro, N.M., Yang, Y., 2007. Processing seismic ambient noise data to obtain reliable broad-band surface wave dispersion measurements. Geophysical Journal International 169, 1239–1260.

Bezacier, L., Reynard, B., Bass, J.D., Sanchez-Valle, C., Van de Moortèle, B., 2010. Elasticity of antigorite, seismic detection of serpentinites, and anisotropy in subduction zones. Earth and Planetary Science Letters 289, 198–208.

Bodin, T., Sambridge, M., Rawlinson, N., Arroucau, P., 2012. Transdimensional tomography with unknown data noise. Geophys J Int 189, 1536–1556. https://doi.org/10.1111/j.1365-246X.2012.05414.x

Christensen, N., 1996. Poisson's ratio and crustal seismology. Journal of Geophysical Research: Solid Earth 101, 3139–3156.

Coney, P.J., Jones, D.L., Monger, J.W., 1980. Cordilleran suspect terranes. Nature 288, 329.

Dziewonski, A.M., Anderson, D.L., 1981. Preliminary reference Earth model. Physics of the earth and planetary interiors 25, 297–356.

Fazlikhani, H., Fossen, H., Gawthorpe, R. L., Faleide, J. I., and Bell, R. E. (2017), Basement structure and its influence on the structural configuration of the northern North Sea rift, Tectonics, 36, 1151– 1177, doi:10.1002/2017TC004514.

Fichtner, A., 2014. Source and processing effects on noise correlations. Geophysical Journal International, 197(3), pp.1527-1531.

Galetti, E., Curtis, A., Baptie, B., Jenkins, D., Nicolson, H., 2016. Transdimensional Love-wave tomography of the British Isles and shear-velocity structure of the East Irish Sea Basin from ambient-noise interferometry. Geophysical Journal International 208, 36–58.

Gibson, G.M., Totterdell, J., Morse, M.P., Goncharov, A., Mitchell, C.H., Stacey, A.R., 2012. Basement Structure and Its Influence on the Pattern and Geometry of Continental Rifting and Breakup Along Australia's Southern Rift Margin. Geoscience Australia.

Heidbach, O., Tingay, M., Barth, A., Reinecker, J., Kurfeß, D., & Müller, B. (2010). Global crustal stress pattern based on the World Stress Map database release 2008. Tectonophysics, 482(1-4), 3–15. doi:10.1016/j.tecto.2009.07.023

Herrmann, R.B., 2013. Computer programs in seismology: An evolving tool for instruction and research. Seismological Research Letters 84, 1081–1088.

Holdsworth, R.E., Stewart, M., Imber, J., Strachan, R.A., 2001. The structure and rheological evolution of reactivated continental fault zones: a review and case study. Geological Society, London, Special Publications 184, 115–137.

Ji, S., Li, A., Wang, Q., Long, C., Wang, H., Marcotte, D., Salisbury, M., 2013. Seismic velocities, anisotropy, and shear-wave splitting of antigorite serpentinites and tectonic implications for subduction zones. Journal of Geophysical Research: Solid Earth 118, 1015–1037.

Kelly, A., England, R.W. and Maguire, P.K.H. (2007), A crustal seismic velocity model for the UK, Ireland and surrounding seas. Geophysical Journal International, 171: 1172-1184. doi:10.1111/j.1365-246X.2007.03569.x

Kennett, B.L., Engdahl, E.R., Buland, R., 1995. Constraints on seismic velocities in the Earth from traveltimes. Geophysical Journal International 122, 108–124.

Klemperer, S.L., 1988. Crustal thinning and nature of extension in the northern North Sea from deep seismic reflection profiling. Tectonics 7, 803–821.

Klemperer, S.L., Hobbs, R., Hobbs, R.W., 1991. The BIRPS Atlas: Deep Seismic Reflections Profiles Around the British Isles. Cambridge University Press.

Kodaira, S., 2004. High Pore Fluid Pressure May Cause Silent Slip in the Nankai Trough. Science 304, 1295–1298. https://doi.org/10.1126/science.1096535

Lecocq, T., Caudron, C., Brenguier, F., 2014. MSNoise, a python package for monitoring seismic velocity changes using ambient seismic noise. Seismological Research Letters 85, 715–726.

Lister, G.S., Etheridge, M.A., Symonds, P.A., 1991. Detachment models for the formation of passive continental margins. Tectonics 10, 1038–1064.

Madsen, L., 1974. Approximate geothermal gradients in Denmark and the Danish North Sea sector. Danm. Geol. Unders. \AArbog for 5–16.

McKenzie, D., 1978. Some remarks on the development of sedimentary basins. Earth and Planetary science letters 40, 25–32.

Milton-Worssell, R., Smith, K., McGrandle, A., Watson, J., Cameron, D., 2010. The search for a Carboniferous petroleum system beneath the Central North Sea. Petroleum Geology Conference series 7, 57–75. https://doi.org/10.1144/0070057

Nicolson, H., Curtis, A., Baptie, B., 2014. Rayleigh wave tomography of the British Isles from ambient seismic noise. Geophysical Journal International 198, 637–655.

Nielsen, L., Balling, N., Jacobsen, B. H., and MONA LISA Working Group (2000). Seismic and gravity modelling of the crustal structure in the Central Graben, North Sea: Observations along MONA LISA profile 3. Tectonophysics, 328, 229-244.

Peacock, S.M., Christensen, N.I., Bostock, M.G., Audet, P., 2011. High pore pressures and porosity at 35 km depth in the Cascadia subduction zone. Geology 39, 471–474.

Pharaoh, T., England, R., Lee, M., 1995. The concealed Caledonide basement of Eastern England and the southern North Sea — A review. Stud Geophys Geod 39, 330–346. https://doi.org/10.1007/BF02295826

Pharaoh, T.C., 1999. Palaeozoic terranes and their lithospheric boundaries within the Trans-European Suture Zone (TESZ): a review. Tectonophysics 314, 17–41. https://doi.org/10.1016/S0040-1951(99)00235-8

Ramachandran, K., Hyndman, R.D., Brocher, T.M., 2006. Regional P-wave velocity structure of the Northern Cascadia Subduction Zone. J. Geophys. Res. 111, n/a-n/a. https://doi.org/10.1029/2005JB004108

Schiffer, C., Doré, A.G., Foulger, G.R., Franke, D., Gernigon, L., Holdsworth, B., Kusznir, N., Lundin, E., Peace, A., Petersen, K.D., Phillips, T., Stephenson, R., Stoker, M.S., Welford, K., 2019. Structural inheritance in the North Atlantic 81.

Schimmel, M., Stutzmann, E., Gallart, J., 2011. Using instantaneous phase coherence for signal extraction from ambient noise data at a local to a global scale. Geophysical Journal International 184, 494–506.

Sissingh, W., 2004. Palaeozoic and Mesozoic igneous activity in the Netherlands: a tectonomagmatic review. Netherlands Journal of Geosciences 83, 113–134.

Smit, J., van Wees, J.D., Cloetingh, S., 2016. The Thor suture zone: From subduction to intraplate basin setting. Geology 44, 707–710. https://doi.org/10.1130/G37958.1

Smithson, S.B., Wenzel, F., Ganchin, Y.V., Morozov, I.B., 2000. Seismic results at Kola and KTB deep scientific boreholes: velocities, reflections, fluids, and crustal composition. Tectonophysics 329, 301–317.

Stratford, W., Thybo, H., Faleide, J.I., Olesen, O. and Tryggvason, A., 2009. New Moho map for onshore southern Norway. Geophysical Journal International, 178(3), pp.1755-1765.

Tesauro, M., Kaban, M.K., Cloetingh, S.A., 2008. EuCRUST-07: A new reference model for the European crust. Geophysical Research Letters 35.

Thybo, H., Maguire, P.K.H., Birt, C., Perchuć, E., 2000. Seismic reflectivity and magmatic underplating beneath the Kenya Rift. Geophysical Research Letters 27, 2745–2748.

Torsvik, T.H., Rehnström, E.F., 2003. The Tornquist Sea and Baltica–Avalonia docking. Tectonophysics 362, 67–82.

Ventosa, S., Schimmel, M., Stutzmann, E., 2017. Extracting surface waves, hum and normal modes: time-scale phase-weighted stack and beyond. Geophysical Journal International 211, 30–44.

Wang, X.-Q., Schubnel, A., Fortin, J., David, E.C., Guéguen, Y., Ge, H.-K., 2012. High Vp/Vs ratio: Saturated cracks or anisotropy effects? Geophysical Research Letters 39. https://doi.org/10.1029/2012GL051742

Wenzel, F., Sandmeier, K.-J., 1992. Geophysical evidence for fluids in the crust beneath the Black Forest, SW Germany. Earth-Science Reviews 32, 61–75.

Wernicke, B., 1985. Uniform-sense normal simple shear of the continental lithosphere. Canadian Journal of Earth Sciences 22, 108–125.

Wessel, P., Smith, W.H., Scharroo, R., Luis, J., Wobbe, F., 2013. Generic mapping tools: improved version released. Eos, Transactions American Geophysical Union 94, 409–410.

Williamson, J.P., Pharaoh, T.C., Banka, D., Thybo, H., Laigle, M., Lee, M.K. Potential field modelling of the Baltica–Avalonia (Thor-Tomquist) suture beneath the southern North Sea, Tectonophysics, 360 (1–4) (2002), pp. 47-60

Wilson, P.I.R., McCaffrey, K.J.W., Wilson, R.W., Jarvis, I., Holdsworth, R.E., 2016. Deformation structures associated with the Trachyte Mesa intrusion, Henry Mountains, Utah: Implications for sill and laccolith emplacement mechanisms. Journal of Structural Geology 87, 30–46. https://doi.org/10.1016/j.jsg.2016.04.001

Yamasaki, T., Gernigon, L., 2009. Styles of lithospheric extension controlled by underplated mafic bodies. Tectonophysics 468, 169–184.

Yang, Y., Ritzwoller, M.H., Levshin, A.L., Shapiro, N.M., 2007. Ambient noise Rayleigh wave tomography across Europe. Geophysical Journal International 168, 259–274.

Yardley, B.W., 1989. An introduction to metamorphic petrology.

Yao, H. and Van Der Hilst, R.D., 2009. Analysis of ambient noise energy distribution and phase velocity bias in ambient noise tomography, with application to SE Tibet. Geophysical Journal International, 179(2), pp.1113-1132.

Young, M.K., Rawlinson, N., Arroucau, P., Reading, A.M., Tkalčić, H., 2011. High-frequency ambient noise tomography of southeast Australia: New constraints on Tasmania's tectonic past. Geophysical Research Letters 38. https://doi.org/10.1029/2011GL047971

Young, M.K., Rawlinson, N., Bodin, T., 2013. Transdimensional inversion of ambient seismic noise for 3D shear velocity structure of the Tasmanian crust. Geophysics 78, WB49–WB62.

Ziegler, P.A., 1990. Geological atlas of western and central Europe. Geological Society of London.

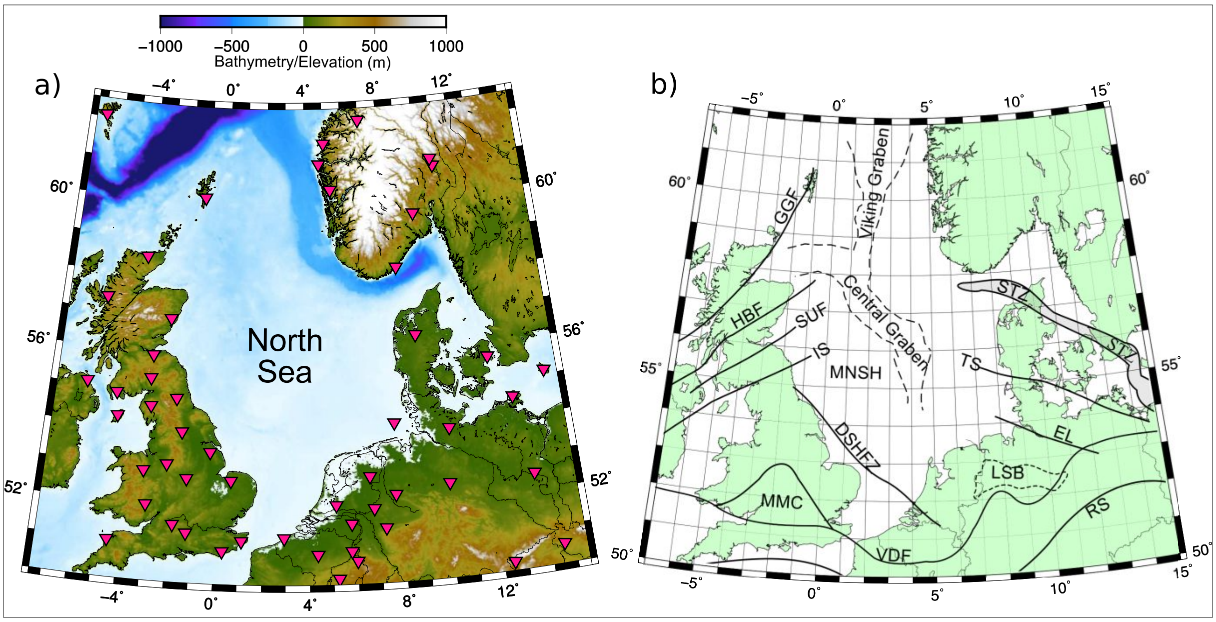

Fig. 1: Map of the North Sea and surrounding regions showing (a) seismometers used in this study (red triangles); and (b) major crustal features in the study area. GGF: Great Glen Fault; HBF: Highland Boundary Fault; SUF: Southern Uplands Fault; IS: Iapetus Suture; MNSH: Mid-North Sea High; DSHFZ: Dowsing South Hewett Fault Zone; MMC: Midlands Micro-craton; VDF: Variscan Deformation Front; LSB: Lower Saxony Basin; RS: Rheic Suture; EL: Elbe Lineament; TS: Thor Suture; STZ: Sorgenfrei-Tornquist Zone.

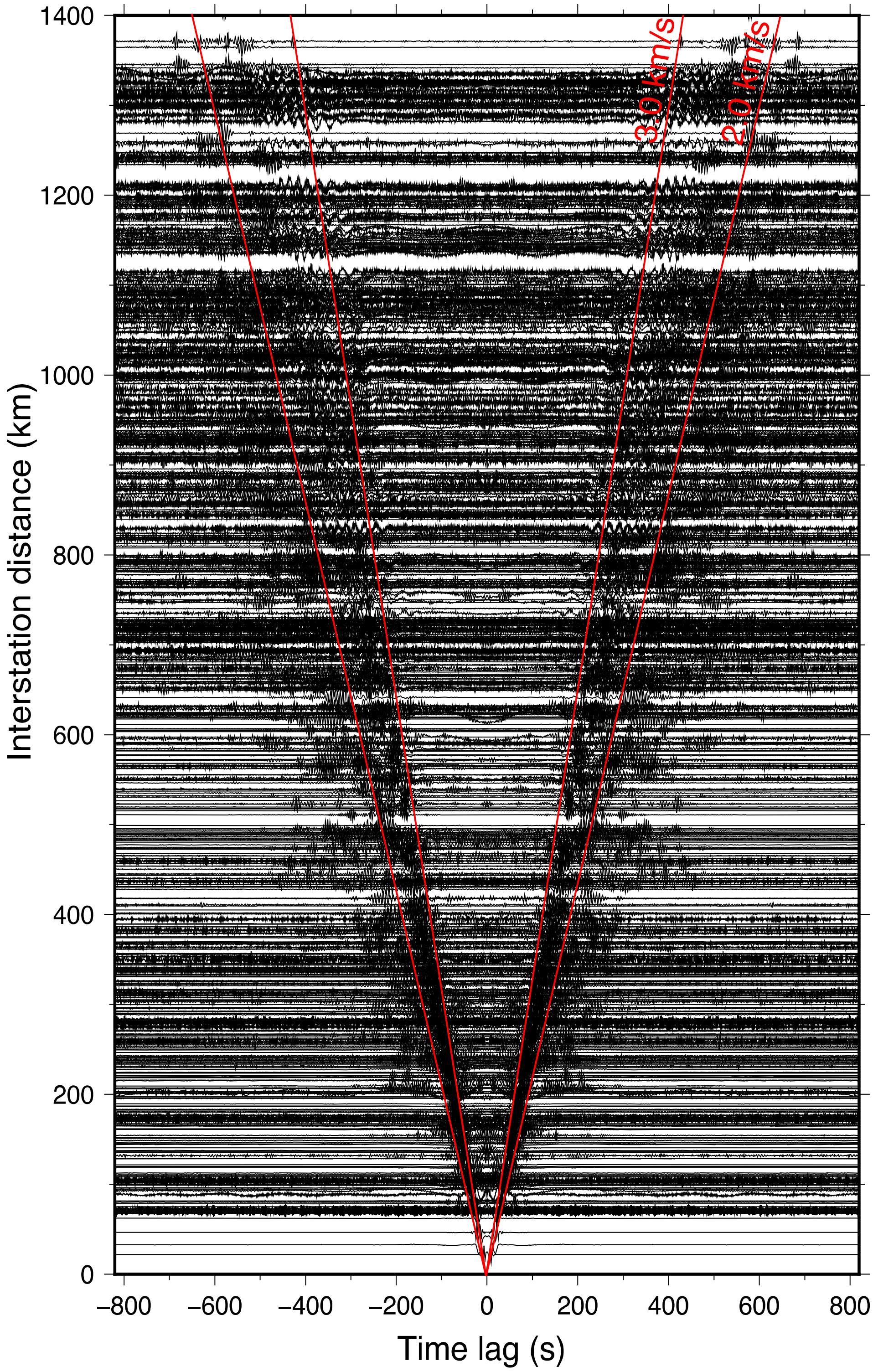

Fig. 2: Final cross-correlations (symmetric component) for all simultaneously recording station pairs used for group velocity dispersion analysis, obtained from phase weighted stacking, plotted as a function of interstation distance. The red lines are plotted to highlight moveout velocities of 2 km/s and 3 km/s.

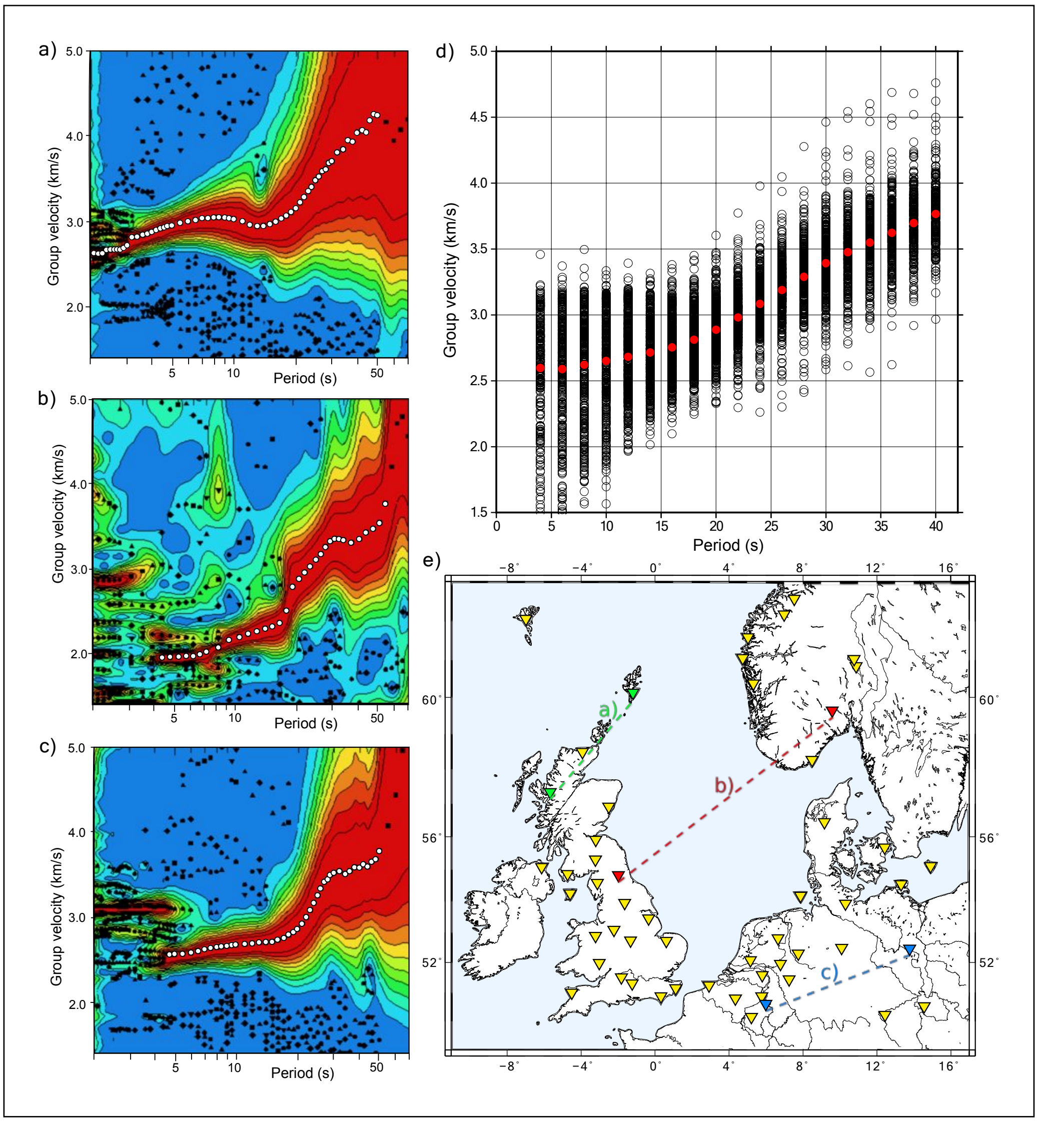

Fig. 3: (a-c) Plots showing group velocity dispersion curves computed from cross-correlations between the three station pairs shown in (e), with white dots denoting the group dispersion picks; (d) dispersion data from all 614 "good" curves, with the average for each period shown in red.

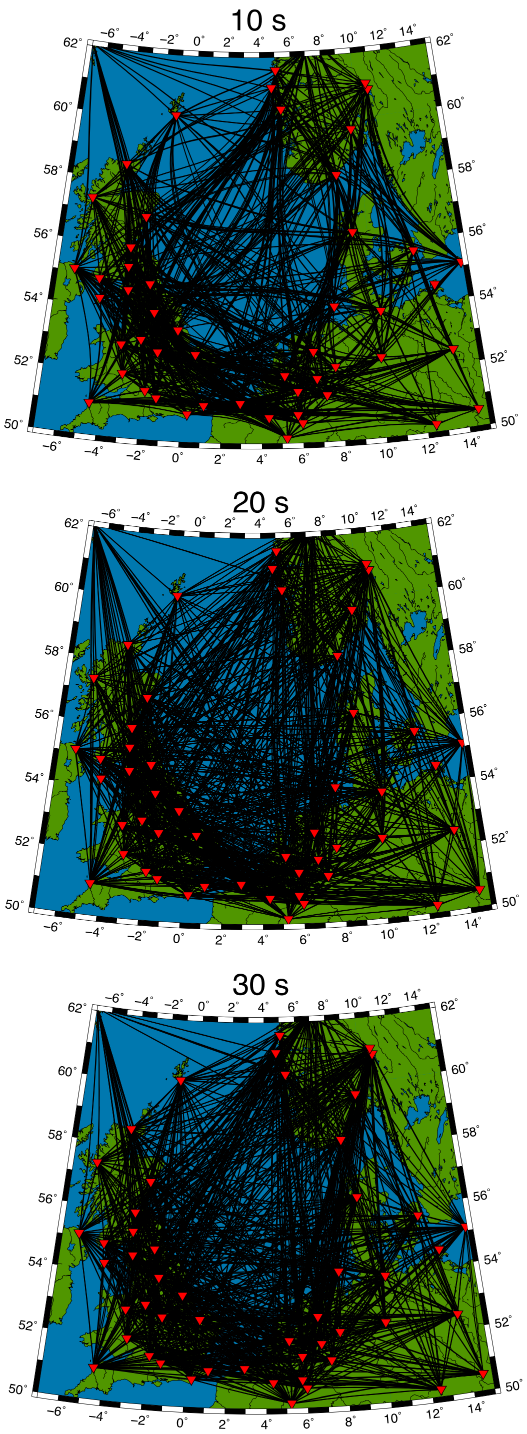

Fig. 4: Ray paths for 10, 20 and 30 s periods, with red triangles showing the location of seismometer stations used in this project.

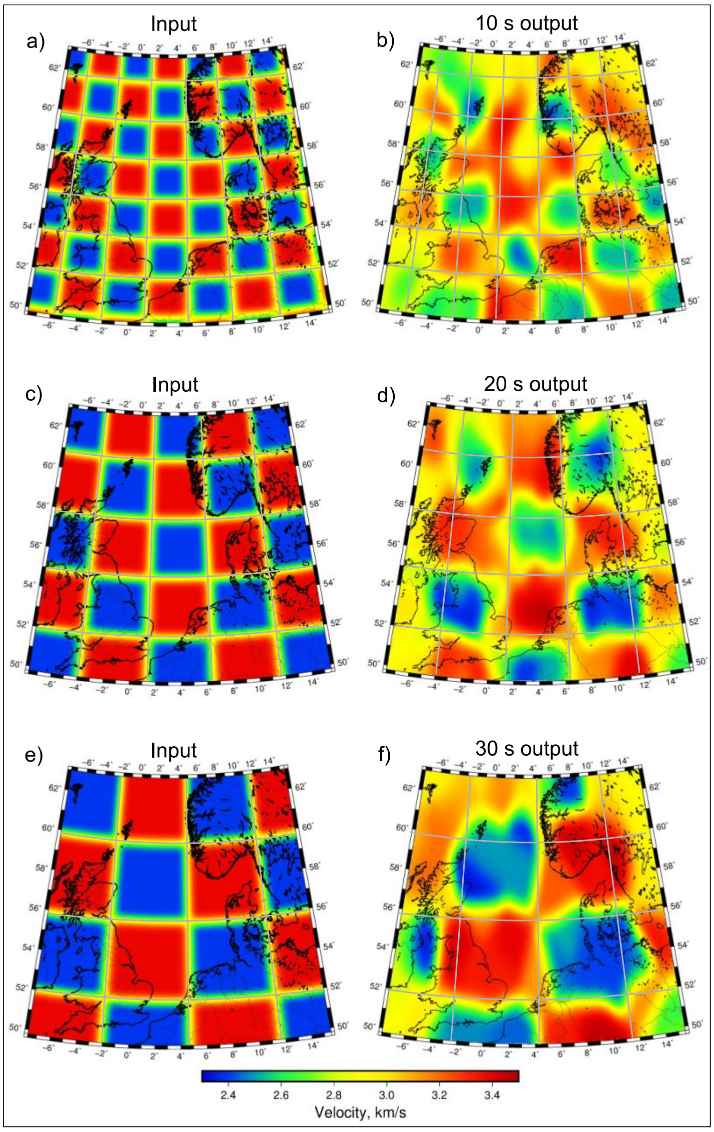

Fig. 5: Checkerboard resolution tests for velocity structure recovery using transdimensional, hierarchical, Bayesian inversion. Synthetic input velocities are input as small, medium and large size checkerboard patterns. Output velocity models (right) for optimum recovery periods. See supplementary Fig. 2 for outputs from all periods. Grey lines overlaid for visual comparison.

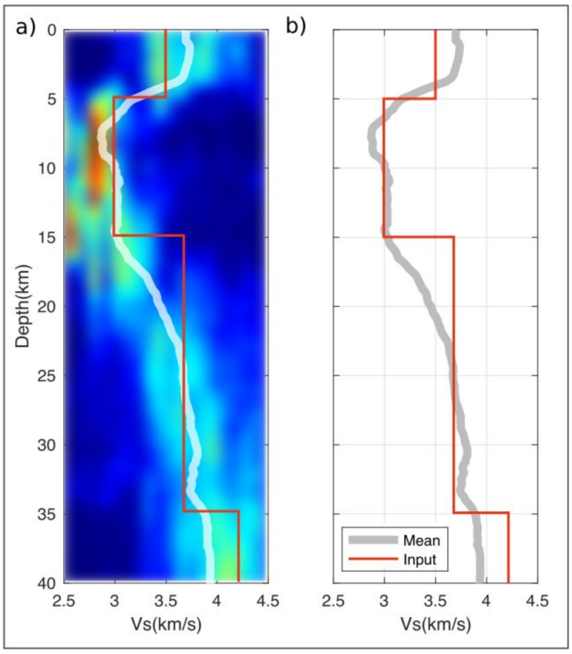

Fig. 6: Results of a synthetic recovery test for 1D crustal shear velocity structure. Red solid line denotes the input model that we attempt to recover. (a) Probability density plot; red is high probability and blue is low probability; (b) mean of the recovered velocity distribution.

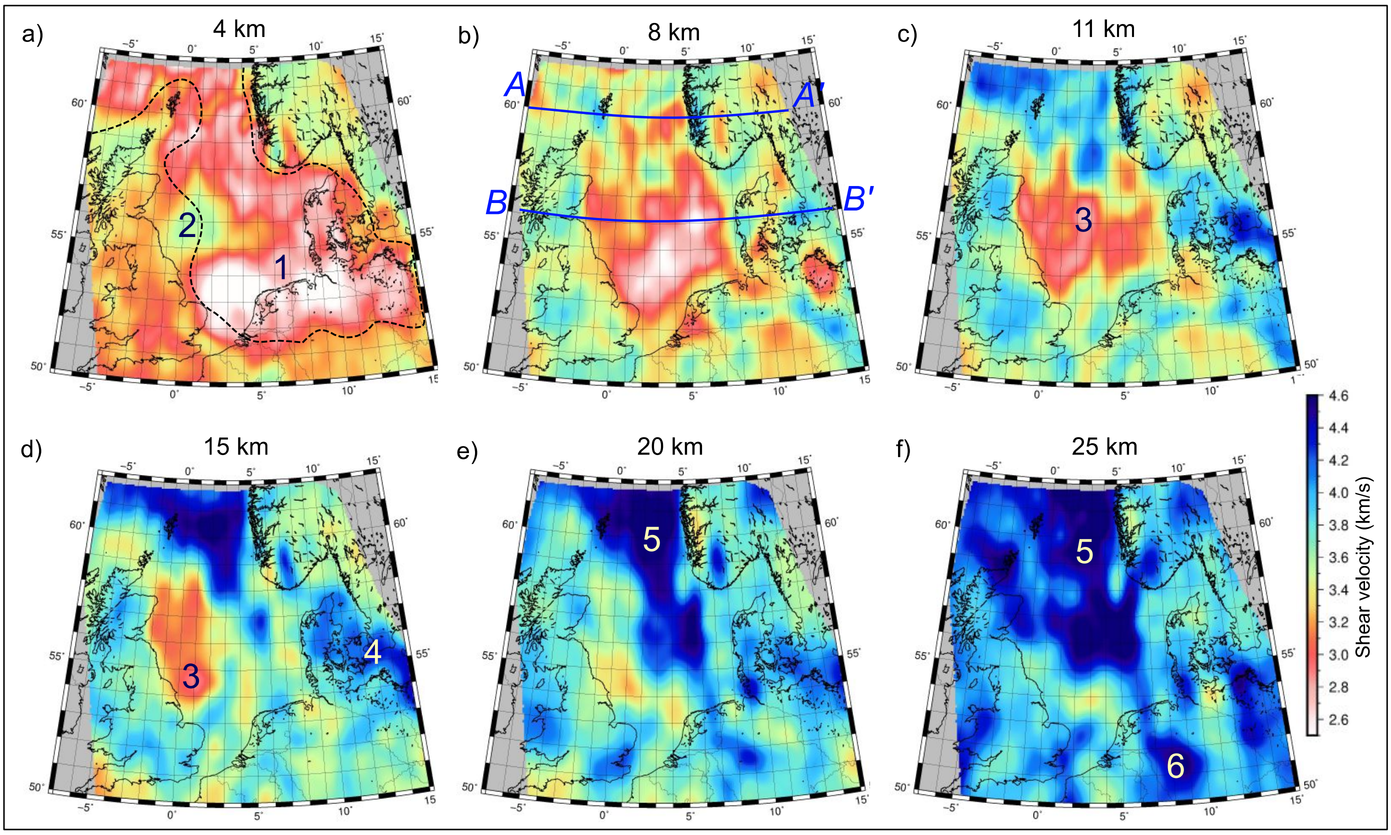

Fig. 7: Depth slices through the new 3D shear-wave velocity model of the North Sea and surrounding landmasses at depths of 4, 8, 11, 15, 20 and 25 km. Labelled velocity anomalies '1-6' are discussed in the text. Dashed black line on (a) marks 4 km sediment thickness contour from EuCRUST-07 (Tesauro et al., 2008). A-A' and B-B' are the location of cross-section slices shown in Figure 6. See Supplementary Fig. 7 for slices at 30, 35 and 40 km depth.

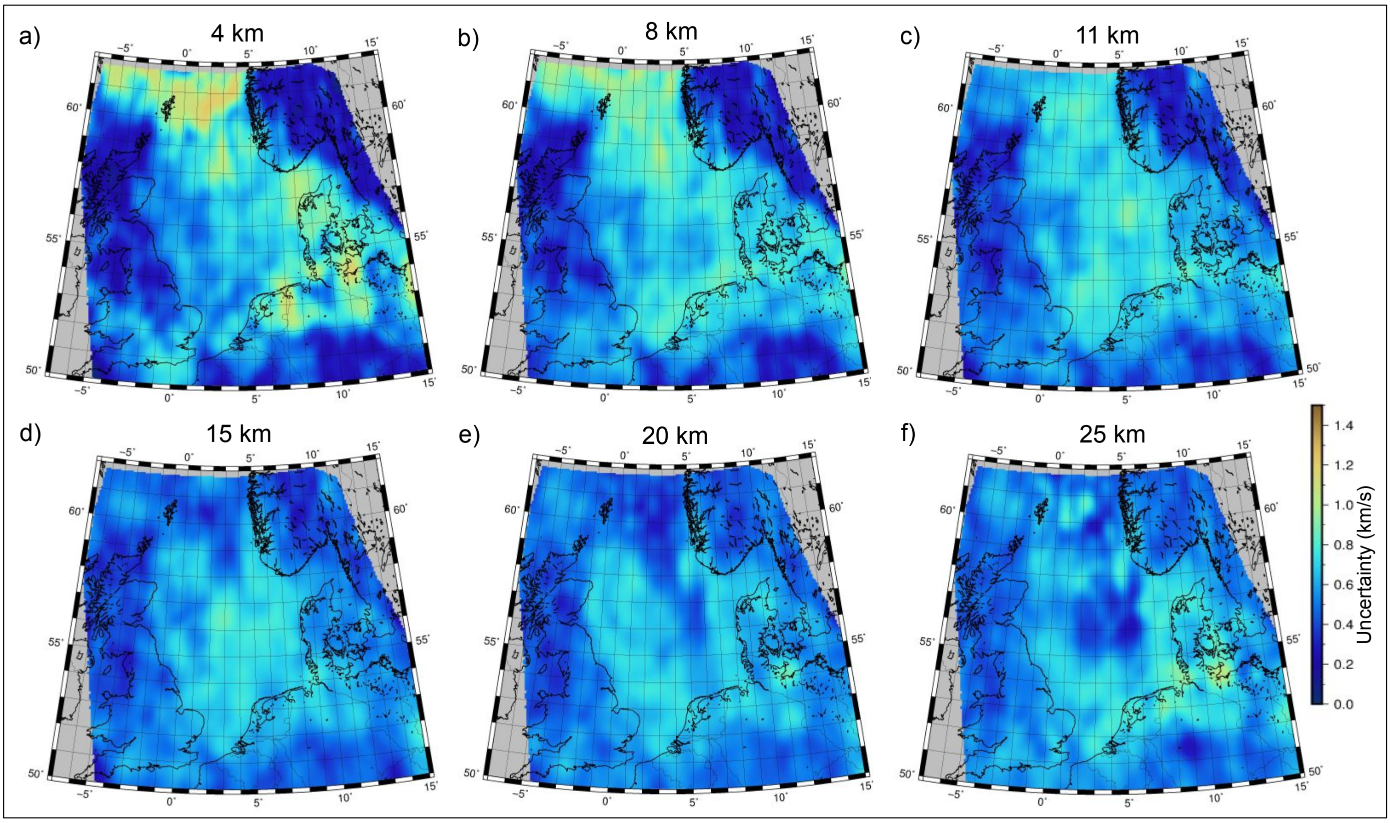

Fig. 8: Associated standard deviation values for the mean velocity model shown in Figure 4. Additional slices at 30, 35 and 40 km depth are shown in Supplementary Fig. 7.

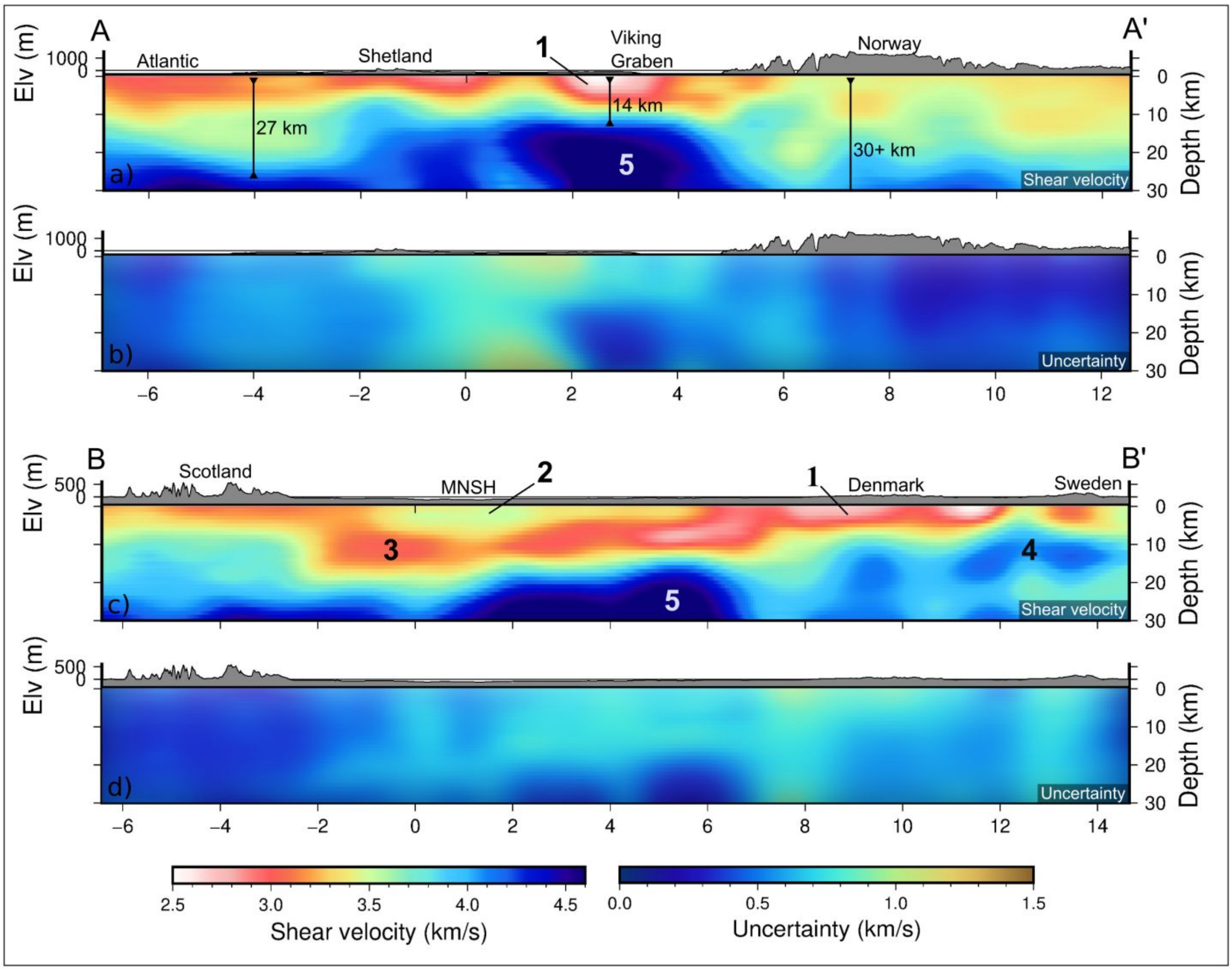

Fig. 9: Cross-section slices through the new 3D shear-wave velocity model of the North Sea and surrounding landmasses at latitudes of 56.0º and 60.0º. Labelled velocity anomalies '1-5' are discussed in the text. Associated standard deviation values for the velocity model are shown below each cross-section. MNSH: Mid North Sea High.

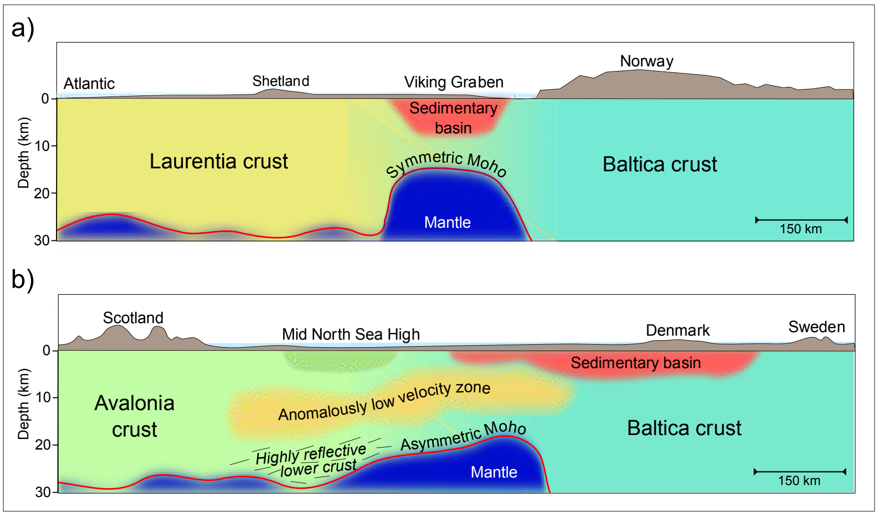

Fig. 10: Cartoon summarising the key interpretations of this study. (a) symmetric thinning of the crust in the northern North Sea between crust of Laurentia and Baltica origin; (b) asymmetric thinning of the crust of Avalonia and Baltica origin with an anomalously low velocity zone above highly seismically reflective lower crust around the Mid North Sea High region.

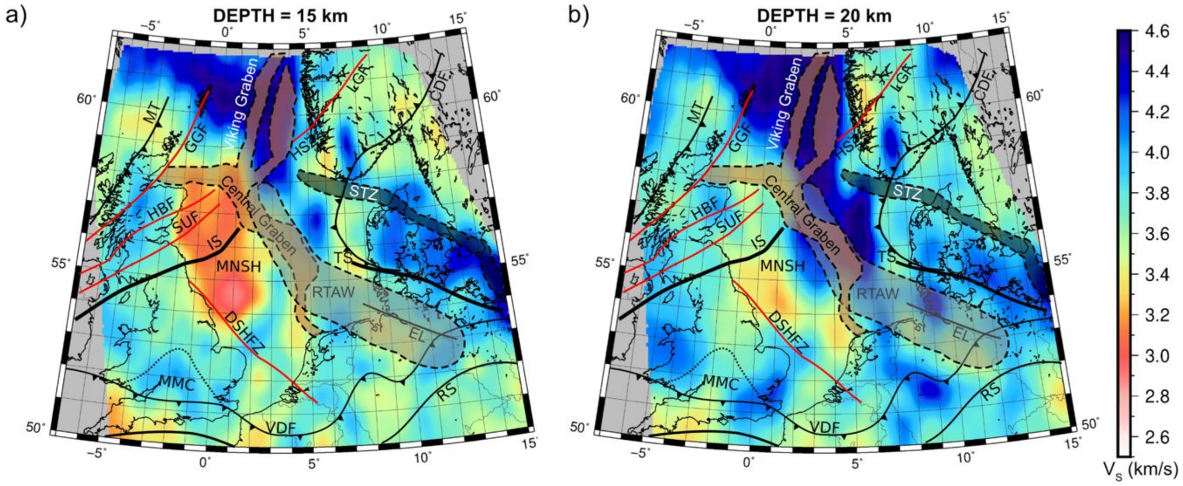

Fig. 11: Major crustal and tectonic features in the study area overlain onto depth slices through the final S-wave velocity model at: a) 15 km; and b) 20 km. MT: Moine Thrust; GGF: Great Glen Fault; HBF: Highland Boundary Fault; SUF: Southern Uplands Fault; IS: Iapetus Suture; MNSH: Mid-North Sea High; DSHFZ: Dowsing South Hewett Fault Zone; MMC: Midlands Micro-Craton; VDF: Variscan Deformation Front; RS: Rheic Suture; EL: Elbe Lineament; TS: Thor Suture;; STZ: Sorgenfrei-Tornquist Zone; HSZ: Hardangerfjord Shear Zone; LGF: Lærdal-Gjende Faults; CDF: Caledonian Deformation Front. The Remnant Thor Accretionary Wedge (RTAW) shaded grey is a low P-wave velocity region (after Smit et al., 2016) and brown shading denotes regions of major Late Palaeozoic-Mesozoic extension (after Fazlikhani et al., 2017).

Supplementary material for:

Controls on the development and termination of failed continental rifts: Insights from the crustal structure and rifting style of the North Sea via ambient noise tomography

E. Crowder[1,*], N. Rawlinson[2], D. G. Cornwell[1], C. Sammarco[1], E. Galetti[4], A. Curtis[3,4]

1. School of Geosciences, University of Aberdeen, Aberdeen AB24 3UE, Scotland, United Kingdom
2. Department of Earth Sciences, University of Cambridge, Cambridge, CB3 0EZ, United Kingdom
3. School of Geosciences, University of Edinburgh, Edinburgh, EH8 9XP, United Kingdom
4. Institute of Geophysics, ETH Zurich, Zurich, Switzerland

* Corresponding author. Email address: emily.crowder@abdn.ac.uk (E. Crowder)

Content of this file:

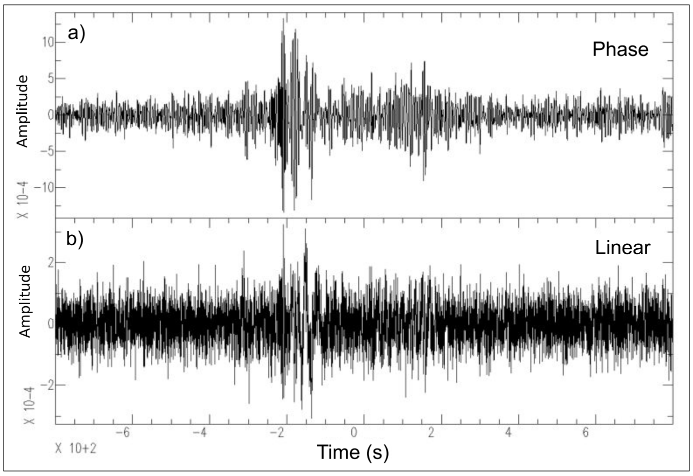

Figure S1: Linear stack of all daily cross-correlations between station pairs EDI and LWR using the phase cross-correlation method in (a) and a linear cross-correlation method with power value 1 in (b).

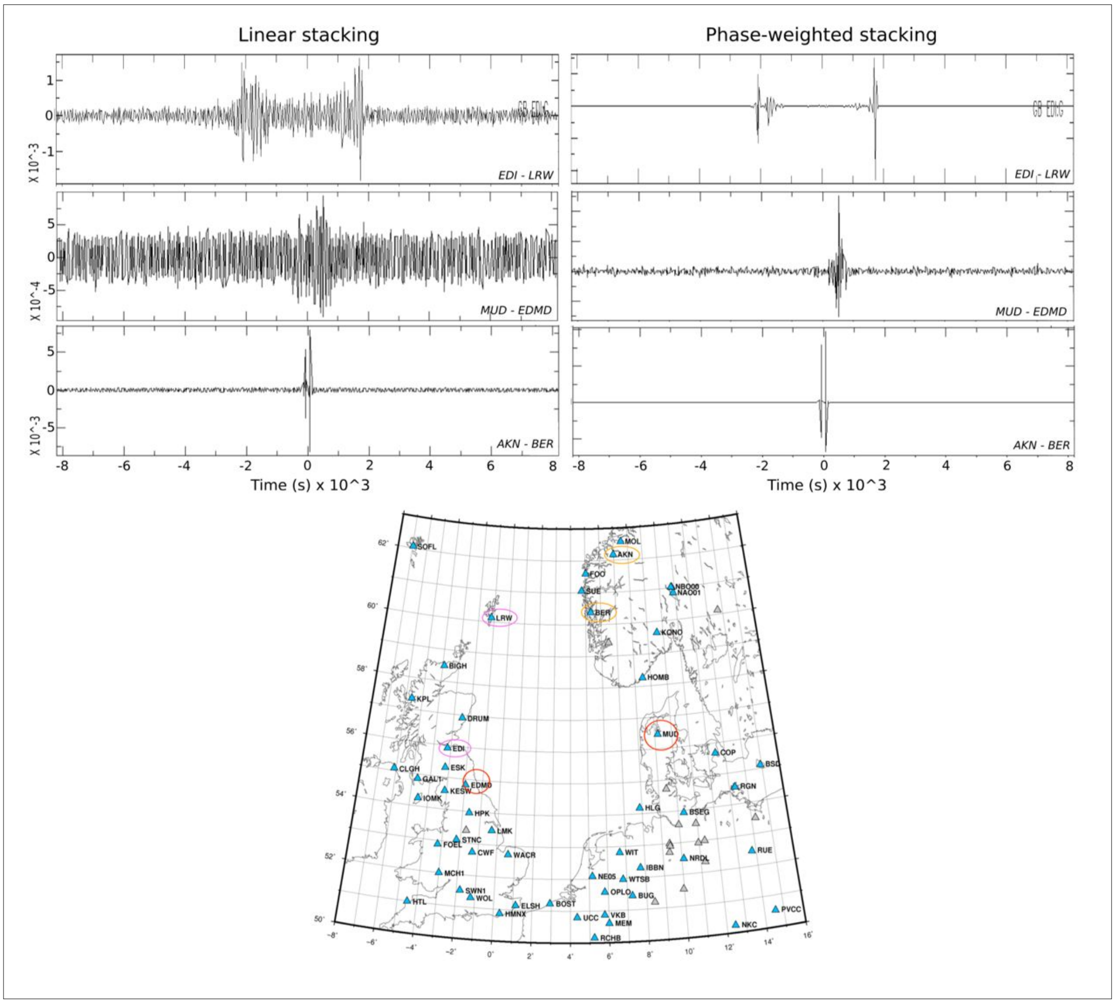

Figure S2: Comparison of linear and phase-weighted stacking methods for three example station pairs. The map below highlights the stations used in this example.

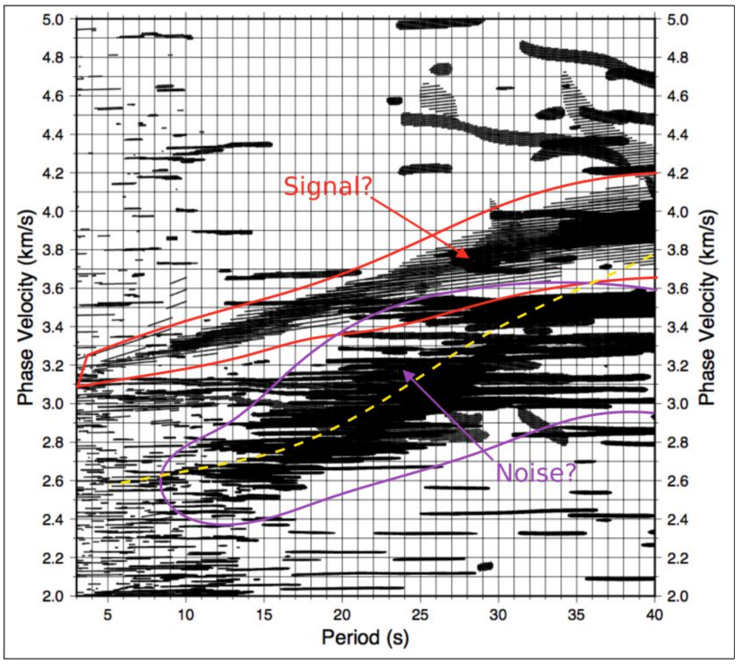

Figure S3: Phase dispersion plot created from automated frequency-time analysis using the image transformation technique. Average group velocity dispersion trend plotted as dashed yellow line for reference. Possible phase velocity signal shown outlined in red, with what may be noise highlighted in purple below.

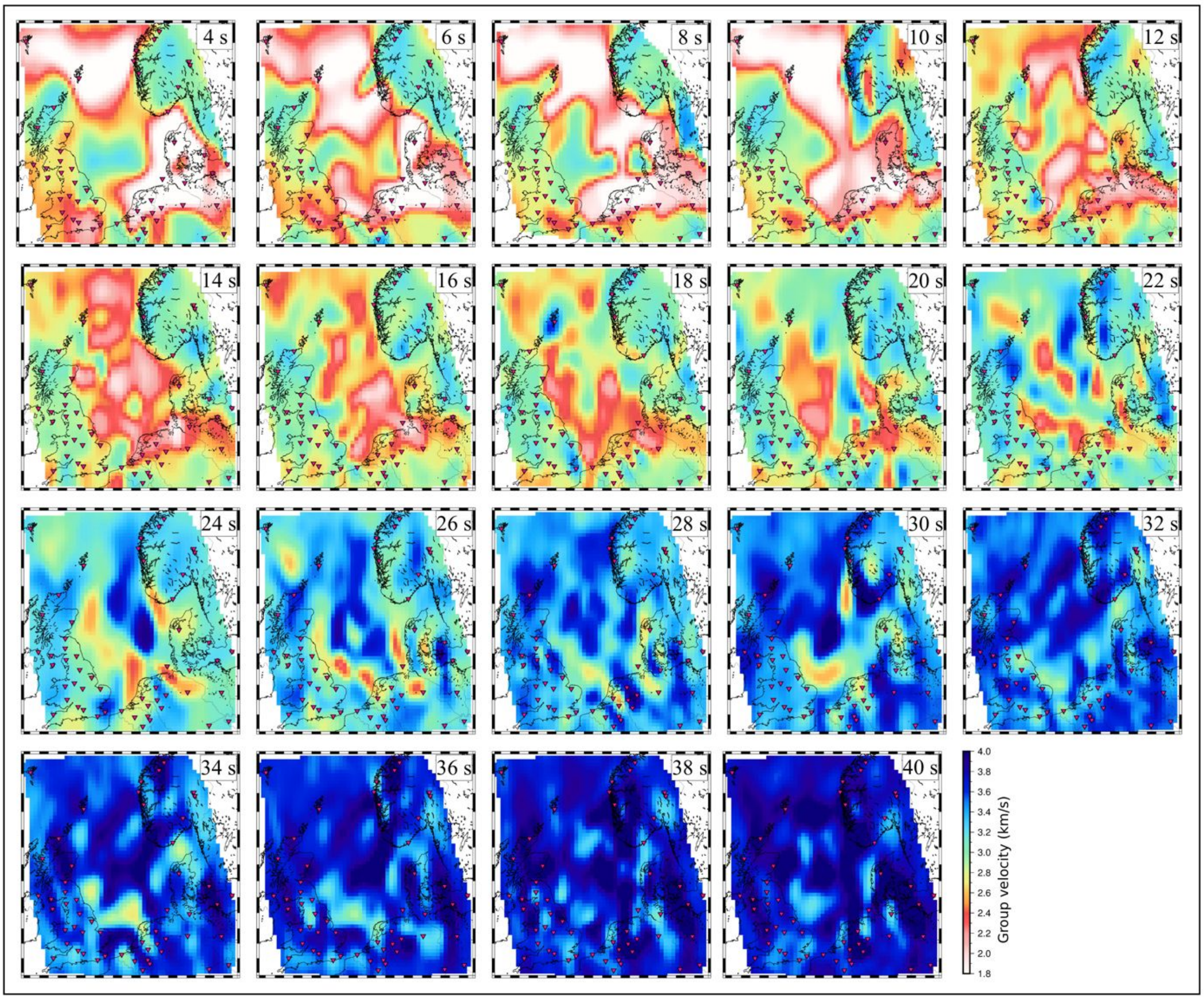

Figure S4: Group velocity maps of the North Sea and surrounding landmasses at even numbered periods from 4 to 40 s. Each pixel is associated with the regular grid of 2,903 points across the study area used to generate pseudo 1D group velocity dispersion curves.

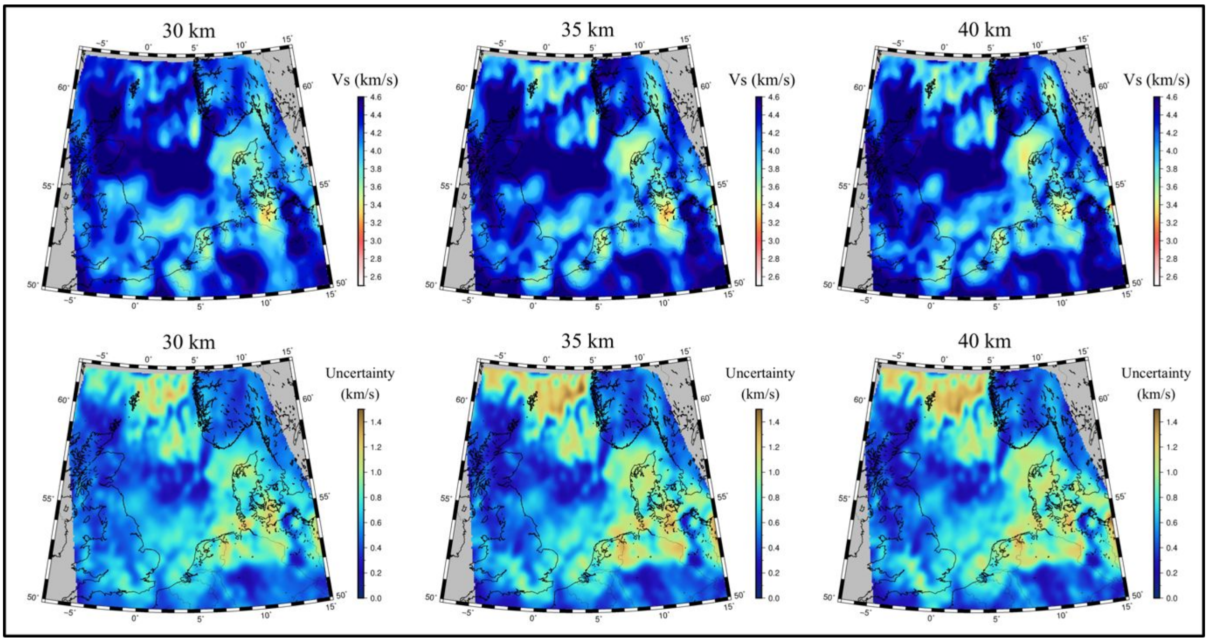

Figure S5: Depth slices taken through our new 3D shear-wave velocity model of the North Sea and surrounding landmasses at depths of 30, 35 and 40 km and their associated uncertainty estimates.

Inversion parameters for tomographic inversions

2D group velocity inversion priors

BURNIN= 100,000
The number of iterations to be discarded

TOTAL= 500,000 ,
The total number of iterations to run (per process in the MPI version)

THIN= 100 ,
Remaining models after burn-in sifted by taking every Nth model

MINPARTITIONS= 10 ,
The minimum number of partitions

MAXPARTITIONS= 400 ,
The maximum number of partitions

INITPARTITIONS= 200 ,
The initial number of partitions

JITTERPARTITIONS= 100 ,
For MPI only, jitter the number of initial partitions about *initpartitions*. in each process, the initial number of partitions will be uniformly distributed between *initpartitions* - *jitterpartitions* and *initpartitions* + *jitterpartitions*.

MINLON= -11.00 ,
Longitude bounds

MAXLON= 17.00 ,
Longitude bounds

MINLAT= 49.00 ,
Latitude bounds

MAXLAT= 63.00 ,
Latitude bounds

PD= 1.500 ,
The standard deviation for random partition moves

VS_MIN= Average velocity for given period + 0.75 km/s ,
Minimum velocity in each cell in km/s

VS_MAX= Average velocity for given period - 0.75 km/s ,
Maximum velocity in each cell in km/h

VS_STD_VALUE= 1.00,

The standard deviation for a change in velocity value
VS_STD_BD= 1.00 ,
For birth/death move, this is the standard deviation of the new cell's velocity value

SIGMA_MIN= 1.00 ,
Minimum value of noise parameter

SIGMA_MAX= 50.00 ,
Maximum value of noise parameter

SIGMA_STD= 1.00 ,
Standard deviation value of noise parameter

The code is open source and can be downloaded from here:
http://www.iearth.org.au/codes/rj-TOMO/